Vehicle's Dynamic Behavior in Fishhook Maneuver by Considering the Engine Dynamics

Ali Shahabi[1], Amir Hossein Kazemian[2, *], Said Farahat[3], Faramarz Sarhaddi[4]
Department of Mechanical Engineering,
University of Sistan and Baluchestan, Iran
E-mail: alishahabi@pgs.usb.ac.ir, kazemian@eng.usb.ac.ir, farahat@hamoon.usb.ac.ir, fsarhaddi@eng.usb.ac.ir
*Corresponding author

Received: 2 January 2021, Revised: 16 April 2021, Accepted: 20 April 2021

Abstract: In order to study on the vehicle's dynamic behavior, this study presents a new dynamic modeling of the vehicle by considering the engine dynamics. The coordinate systems are considered separately for the sprung mass and unsprung masses. By using Newton's equations of motion, the force-torque equations of the sprung mass and unsprung masses are derived in the vehicle coordinate system. In general, the sprung mass in modeling of the vehicle is considered as a rigid body. However, in this study the components rotation of the sprung mass such as the engine crankshaft is considered and its gyroscopic effects are exerted in the governing equations. The lateral and longitudinal forces of the tire are evaluated by Pacejka model. In fishhook maneuver, the vehicle's dynamic behavior is studied by the numerical simulation method under the supervision of the National Highway Traffic Safety Administration (NHTSA). The numerical simulation results are also validated by ADAMS/Car software. According to the results, the 15-DOF model in this research simulates the vehicle's dynamic behavior with a good accuracy and the maximum roll rate of the vehicle reaches about 37 degrees per second.

Keywords: Crankshaft, Gyroscopic Effects, Pacejka Model, Vehicle Coordinate System

How to cite this paper: Ali Shahabi, Amir Hossein Kazemian, Said Farahat, and Faramarz Sarhaddi, "Vehicle's Dynamic Behavior in Fishhook Maneuver by Considering the Engine Dynamics" , Int J of Advanced Design and Manufacturing Technology, Vol. 14/No. 2, 2021, pp. 23–35.
DOI: 10.30495/admt.2021.1919552.1237

Biographical notes: Ali Shahabi is a PhD student in Mechanical Engineering at University of Sistan and Baluchestan, Zahedan, Iran. His current research interest includes suspension and gear systems and vehicle dynamics. **Amir Hossein Kazemian** is currently Assistant Professor of Mechanical engineering at University of Sistan and Baluchestan and his current research focuses on vehicle dynamics. **Said Farahat** is Professor of Mechanical engineering at University of Sistan and Baluchestan and his current research focuses on renewable energy. **Faramarz Sarhaddi** is currently Associate Professor of Mechanical engineering at University of Sistan and Baluchestan and his main research interests are solar collector and HDH system.

1 INTRODUCTION

Vehicle safety has always been very important to vehicle designers. Nowadays, vehicles have to meet stringent safety standards in order to be allowed to enter the market. Vehicle stability is one of the most important issues in pre-crash safety, and knowing the dynamic behavior of the vehicle in standard maneuvers can be effective in assessing vehicle stability. For this purpose, in order to achieve real results, a comprehensive model of the vehicle dynamics is always needed.

A set of experimental examinations was performed to evaluate the actual dynamic behavior of the vehicle in various standard maneuvers [1] which can be pointed out the phase IV rollover tests of the NHTSA [2]. Nalecz et al. [3] tested eight vehicles of different types in rollover maneuvers. These maneuvers include the maneuvers in which the driver loses control of the vehicle and the vehicle deviates toward the perimeter of the road. The modeling presented by Allen et al. [4] was performed by considering the fixed roll axis, which was modified and validated based on the test results. Zulhilmi et al. [5] analyzed the vehicle's dynamic behavior during emergency braking on wet and dry surface condition by an experimental study. Ahmadian [6] improved vehicle handling, stability, and ride comfort and also Ataei et al. [7] studied on the lateral stability and rollover prevention of the vehicle. Phanomchoeng and Rajamani [8] developed a new rollover index that can detect both tripped and untripped rollovers by experimental and simulation examinations. The purpose of computer simulations is to reveal the effect of systems and components on the dynamic behavior of the vehicle as much as possible. By using computer simulations, these purposes can be performed much earlier in the targeting and initial design stages of the vehicle than the actual prototype. Peng et al. [9] studied on the lateral and longitudinal tire forces of the full-car model by computer simulations. Yuvapriya et al. [10] examined the suspension system and dynamic behavior of the vehicle in order to simulate the vehicle stability. Papaioannou et al. [11] compared four vehicle models with various configurations in order to study on the vehicle's dynamic behavior such as ride comfort, vehicle handling and road holding by computer simulations. Mehrtash et al. [12] simulated the normal force of tires and roll angle of the vehicle under hand-wheel angle sequences for NHTSA fishhook maneuver. Wang and Chen [13] designed the active rollover preventer to enhance the performance of vehicle rollover in fishhook maneuver by computer simulations. Zhang et al. [14] simulated a 7-DOF model of the vehicle and they analyzed the yaw rate in order to improve the vehicle handling. Read and Viswanathan [15] investigated the effects of induced pressure loads from a realistic vehicle onto the surface of a road-side wall by using numerical simulation. Rajamani [16] and Gillespie [17] studied on the vehicle dynamics and its subsystems such as tire in order to study on the vehicle's dynamic behavior by considering the basics of the dynamic [18]. Pacejka [19-22] examined the tire characteristics such as its longitudinal and lateral forces and obtained the data by mathematical expressions on the basis of a formula. In vehicles, the engine dynamics can be effective in the vehicle simulation. As an example, knowing the dynamic behavior of the engine elements such as crankshaft can be useful for obtaining the dynamic behavior of the vehicle [23-25]. Mourelatos [26] described a system model for analyzing the dynamic behavior of an internal combustion engine crankshaft. A numerical model using an explicit formulation was developed by Fonseca and de Faria [27] in order to accurately simulate crank shaft deep rolling dynamics. Drab et al. [28] simulated the crankshaft dynamics by flexible bodies and force laws describing the interaction between the bodies.

This study by presenting a 15-DOF model of the vehicle dynamics, considers the vehicle modeling that can simulate the vehicle's dynamic behavior in the state of stability threshold of the vehicle and can apply effective design parameters in the model. The tire is modeled with the Pacejka 89 model, which calculates the tire forces using longitudinal and lateral slips. The gyroscopic moment of the crankshaft is directly added to the torque vector of external forces, and the final equations of motion of the vehicle will be extracted. The dynamic behavior of the 15-DOF presented model is validated by ADAMS/Car software. By using numerical method of the Newmark [29], dynamic behavior of the vehicle in fishhook maneuver is simulated under the supervision of the phase IV of NHTSA's light vehicle rollover research program.

2 MODELING AND EQUATIONS

In this research, the vehicle is considered as a set of lumped masses including the sprung mass and four unsprung masses as a set of wheels and tires. The unsprung masses are connected to the sprung mass by the spring and damper. Each tire is assumed equivalent to a spring and a damper in parallel in the vertical direction. The number of degrees of freedom considered for the vehicle model is 15 degrees, which is 6-DOF related to the translation and the rotation of the sprung mass. 4-DOF is for vertical movement of the unsprung masses, which indicates the vertical movement of the suspension systems. 4-DOF is related to the rotation of the wheels around its axis and 1-DOF is considered for steerability of the front wheels. For this set of masses, separate coordinate systems such as fixed inertial coordinate system (O), sprung mass coordinate system (S), roll axis coordinate system (vehicle coordinates (V))

and wheel coordinate system (US) are considered. The direction of the coordinate systems as shown in "Fig. 1" is in accordance with the SAE (Society of Automotive Engineers) standard [17].

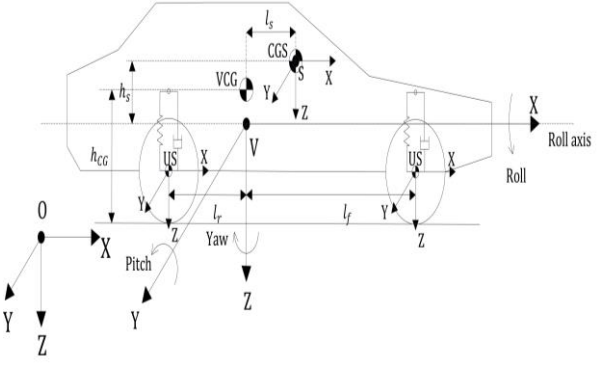

Fig. 1 Direction of the vehicle coordinate system according to the SAE standard.

In "Fig. 1", the sprung mass coordinate system is located at the center of gravity of the sprung mass (CGS). The coordinate system located on the roll axis, which is the most important coordinate system and all variables are expressed in this system, is located at a point on the roll axis and below the center of gravity of the vehicle mass (VCG). It is also assumed that this coordinate system only rotates around the Z axis. To obtain the equations of wheels' motion in the vertical direction and around their rotation axis, for each wheel a coordinate system is used at the center of rotation. According to coordinate systems and using Newton's equations of motion, all equations of motion for the sprung and unsprung masses will be obtained in the vehicle coordinate system. Therefore, for sprung mass, "Eqs. (1-3)" can be written:

$$
\begin{aligned}
&{}^{V}\mathbf{V}_{V}=\left\{V_x \quad V_y \quad 0\right\}^{T},\ {}^{V}\boldsymbol{\omega}_{V}=\left\{0 \quad 0 \quad \dot{\varphi}\right\}^{T}\\
&{}^{V}\boldsymbol{\rho}_{CGS}=\left\{l_s \quad 0 \quad h_s\right\}^{T}\\
&{}^{V}\mathbf{V}_{CGS}=\left\{V_x \quad V_y \quad V_z\right\}^{T}=\left\{V_x \quad V_y \quad \dot{Z}_{CGS}\right\}^{T}
\end{aligned}
\tag{1}
$$

$$
\begin{aligned}
&{}^{V}\boldsymbol{\omega}_{S}=\left\{\dot{\theta}\cos\psi \quad \dot{\psi}\cos\theta \quad \dot{\varphi}+\dot{\psi}\sin\theta+\dot{\theta}\sin\psi\right\}^{T}\\
&{}^{V}\boldsymbol{\omega}_{S}=\left\{\dot{\theta} \quad \dot{\psi}\cos\theta \quad \dot{\varphi}+\dot{\psi}\sin\theta\right\}^{T}\\
&\xrightarrow[\cos\psi=1]{\sin\psi=\psi=0}
\end{aligned}
\tag{2}
$$

$$
\begin{aligned}
&{}^{V}\mathbf{V}_{S}={}^{V}\mathbf{V}_{CGS}+{}^{V}\boldsymbol{\omega}_{S}\times{}^{V}\boldsymbol{\rho}_{CGS}\rightarrow\\
&{}^{V}\mathbf{V}_{S}=\begin{Bmatrix} V_x+h_s\dot{\psi}\cos\theta\\ V_y-h_s\dot{\theta}+l_s\left(\dot{\varphi}+\dot{\psi}\sin\theta\right)\\ \dot{Z}_{CGS}-l_s\dot{\psi}\cos\theta \end{Bmatrix}
\end{aligned}
\tag{3}
$$

Similarly, for unsprung masses, "Eqs. (4-6)" are obtained:

$$
\begin{aligned}
&{}^{V}\boldsymbol{\omega}_{usfR}=\left\{\omega_w\sin\delta_{fR} \quad \omega_w\cos\delta_{fR} \quad \dot{\varphi}\right\}^{T}\\
&{}^{V}\boldsymbol{\omega}_{usfL}=\left\{\omega_w\sin\delta_{fL} \quad \omega_w\cos\delta_{fL} \quad \dot{\varphi}\right\}^{T}\\
&{}^{V}\boldsymbol{\omega}_{usrL}=\left\{0 \quad \omega_w \quad \dot{\varphi}\right\}^{T},\ {}^{V}\boldsymbol{\omega}_{usrR}=\left\{0 \quad \omega_w \quad \dot{\varphi}\right\}^{T}\\
&{}^{V}\mathbf{V}_{CGusij}=\left\{V_x \quad V_y \quad \dot{Z}_{usij}\right\}^{T}
\end{aligned}
\tag{4}
$$

$$
\begin{aligned}
&{}^{V}\boldsymbol{\rho}_{usfR}=\left\{l_f \quad t/2 \quad Z_{usfR}\right\}^{T},\\
&{}^{V}\boldsymbol{\rho}_{usfL}=\left\{l_f \quad -t/2 \quad Z_{usfL}\right\}^{T}\\
&{}^{V}\boldsymbol{\rho}_{usrL}=\left\{l_r \quad -t/2 \quad Z_{usrL}\right\}^{T},\\
&{}^{V}\boldsymbol{\rho}_{usrR}=\left\{l_r \quad t/2 \quad Z_{usrR}\right\}^{T}
\end{aligned}
\tag{5}
$$

$$
\begin{aligned}
&{}^{V}\mathbf{V}_{CGusij}={}^{V}\mathbf{V}_{CGusij}+{}^{V}\boldsymbol{\omega}_{usij}\times{}^{V}\boldsymbol{\rho}_{CGusij}\rightarrow\\
&{}^{V}\mathbf{V}_{usfR}=\begin{Bmatrix} V_x+(Z_{usfR}\omega_w\cos\delta_{fR})-(t/2)\dot{\varphi}\\ V_y-(Z_{usfR}\omega_w\sin\delta_{fR})+l_f\dot{\varphi}\\ \dot{Z}_{usfR}+\omega_w\left((t/2)\sin\delta_{fR}-l_f\cos\delta_{fR}\right)\end{Bmatrix}\\
&{}^{V}\mathbf{V}_{usfL}=\begin{Bmatrix} V_x+(Z_{usfL}\omega_w\cos\delta_{fL})+(t/2)\dot{\varphi}\\ V_y-(Z_{usfL}\omega_w\sin\delta_{fL})+l_f\dot{\varphi}\\ \dot{Z}_{usfL}-\omega_w\left((t/2)\sin\delta_{fL}+l_f\cos\delta_{fL}\right)\end{Bmatrix}\\
&{}^{V}\mathbf{V}_{usrL}=\begin{Bmatrix} V_x+Z_{usrL}\omega_w+(t/2)\dot{\varphi}\\ V_y+l_r\dot{\varphi}\\ \dot{Z}_{usrL}-\omega_w l_r\end{Bmatrix}\\
&{}^{V}\mathbf{V}_{usrR}=\begin{Bmatrix} V_x+Z_{usrR}\omega_w-(t/2)\dot{\varphi}\\ V_y+l_r\dot{\varphi}\\ \dot{Z}_{usrR}-\omega_w l_r\end{Bmatrix}
\end{aligned}
\tag{6}
$$

By placing velocities of "Eqs. (1-3)" in Newton's linear momentum equation of sprung mass, the force vector of sprung mass in the vehicle coordinate system is obtained as "Eq. (7)":

$$
\begin{aligned}
&{}^{V}\mathbf{F}_{S}=m_S\left[\frac{d}{dt}{}^{V}\mathbf{V}_{S}+{}^{V}\boldsymbol{\omega}_{V}\times{}^{V}\mathbf{V}_{S}\right]\rightarrow\\
&{}^{V}\mathbf{F}_{S}=m_S\begin{Bmatrix} \dot{V}_x+h_s(\ddot{\psi}\cos\theta-\dot{\psi}\dot{\theta}\sin\theta)-\dot{\varphi}\left(V_y-h_s\dot{\theta}+l_s\left(\dot{\varphi}+\dot{\psi}\sin\theta\right)\right)\\ \dot{V}_y-h_s\ddot{\theta}+l_s\left(\ddot{\varphi}+\ddot{\psi}\sin\theta+\dot{\psi}\dot{\theta}\cos\theta\right)+\dot{\varphi}\left(V_x+h_s\dot{\psi}\cos\theta\right)\\ \ddot{Z}_{CGS}-l_s(\ddot{\psi}\cos\theta+\dot{\psi}\dot{\theta}\sin\theta)\end{Bmatrix}
\end{aligned}
\tag{7}
$$

Similarly, for unsprung masses, "Eqs. (8-12)" are obtained:

$$ {}^{V}\mathbf{F}_{usij} = m_{usij}\left[\frac{d}{dt}{}^{V}\mathbf{V}_{usij} + {}^{V}\boldsymbol{\omega}_{V}\times{}^{V}\mathbf{V}_{usij}\right] \quad (8) $$

$$ {}^{V}\mathbf{F}_{usfR} = m_{usfR}\begin{Bmatrix} \dot{V}_x + \cos\delta_{fR}\left(\dot{Z}_{usfR}\omega_w + Z_{usfR}\dot{\omega}_w\right) - (t/2)\ddot{\varphi} - \\ \dot{\varphi}\left(V_y - Z_{usfR}\omega_w\sin\delta_{fR} + l_f\dot{\varphi}\right) \\ \dot{V}_y - \sin\delta_{fR}\left(\dot{Z}_{usfR}\omega_w + Z_{usfR}\dot{\omega}_w\right) + l_f\ddot{\varphi} + \\ \dot{\varphi}\left(V_x + Z_{usfR}\omega_w\cos\delta_{fR} - (t/2)\dot{\varphi}\right) \\ \ddot{Z}_{usfR} + \dot{\omega}_w\left((t/2)\sin\delta_{fR} - l_f\cos\delta_{fR}\right) \end{Bmatrix} \quad (9) $$

$$ {}^{V}\mathbf{F}_{usfL} = m_{usfL}\begin{Bmatrix} \dot{V}_x + \cos\delta_{fL}\left(\dot{Z}_{usfL}\omega_w + Z_{usfL}\dot{\omega}_w\right) + (t/2)\ddot{\varphi} - \\ \dot{\varphi}\left(V_y - Z_{usfL}\omega_w\sin\delta_{fL} + l_f\dot{\varphi}\right) \\ \dot{V}_y - \sin\delta_{fL}\left(\dot{Z}_{usfL}\omega_w + Z_{usfL}\dot{\omega}_w\right) + l_f\ddot{\varphi} + \\ \dot{\varphi}\left(V_x + Z_{usfL}\omega_w\cos\delta_{fL} + (t/2)\dot{\varphi}\right) \\ \ddot{Z}_{usfL} - \dot{\omega}_w\left((t/2)\sin\delta_{fL} + l_f\cos\delta_{fL}\right) \end{Bmatrix} \quad (10) $$

$$ {}^{V}\mathbf{F}_{usrL} = m_{usrL}\begin{Bmatrix} \dot{V}_x + \dot{Z}_{usrL}\omega_w + Z_{usrL}\dot{\omega}_w + (t/2)\ddot{\varphi} - \dot{\varphi}\left(V_y + l_r\dot{\varphi}\right) \\ \dot{V}_y + l_r\ddot{\varphi} + \dot{\varphi}\left(V_x + Z_{usrL}\omega_w + (t/2)\dot{\varphi}\right) \\ \ddot{Z}_{usrL} - \dot{\omega}_w l_r \end{Bmatrix} \quad (11) $$

$$ {}^{V}\mathbf{F}_{usrR} = m_{usrR}\begin{Bmatrix} \dot{V}_x + \dot{Z}_{usrR}\omega_w + Z_{usrR}\dot{\omega}_w - (t/2)\ddot{\varphi} - \dot{\varphi}\left(V_y + l_r\dot{\varphi}\right) \\ \dot{V}_y + l_r\ddot{\varphi} + \dot{\varphi}\left(V_x + Z_{usrR}\omega_w - (t/2)\dot{\varphi}\right) \\ \ddot{Z}_{usrR} - \dot{\omega}_w l_r \end{Bmatrix} \quad (12) $$

According to "Eq. (13)", the total forces acting on the vehicle include the forces acting on sprung and unsprung masses:

$$ {}^{V}\mathbf{F}_{V} = {}^{V}\mathbf{F}_{S} + {}^{V}\mathbf{F}_{usij} \rightarrow $$

$$ {}^{V}\mathbf{F}_{V} = \begin{Bmatrix} m\dot{V}_x - m\dot{\varphi}V_y + m_s[h_s(\ddot{\psi}\cos\theta - \dot{\psi}\dot{\theta}\sin\theta + \\ \dot{\varphi}\dot{\theta}) - l_s(\dot{\varphi}\dot{\psi}\sin\theta + \dot{\varphi}^2)] + m_{usf}[\cos\delta_f(\omega_w\left(\dot{Z}_{usfR} + \dot{Z}_{usfL}\right) + \\ \dot{\omega}_w\left(Z_{usfR} + Z_{usfL}\right)) + \dot{\varphi}\omega_w\sin\delta_f\left(Z_{usfR} + Z_{usfL}\right) - 2\dot{\varphi}^2 l_f] + \\ m_{usr}[\omega_w\left(\dot{Z}_{usrR} + \dot{Z}_{usrL}\right) + \dot{\omega}_w\left(Z_{usrR} + Z_{usrL}\right) + \\ -2\dot{\varphi}^2 l_r] \\ \\ m\dot{V}_y + m\dot{\varphi}V_x - m_s[h_s(\ddot{\theta} - \dot{\varphi}\dot{\psi}\cos\theta) + l_s(\ddot{\varphi} - \\ \ddot{\psi}\sin\theta - \dot{\theta}\dot{\psi}\cos\theta)] + m_{usf}[-\sin\delta_f(\omega_w\left(\dot{Z}_{usfR} + \dot{Z}_{usfL}\right) + \\ \dot{\omega}_w\left(Z_{usfR} + Z_{usfL}\right)) + 2\ddot{\varphi}l_f + \dot{\varphi}\omega_w\cos\delta_f(Z_{usfR} + \\ Z_{usfL})] + m_{usr}[\dot{\varphi}\omega_w\left(Z_{usrR} + Z_{usrL}\right) + 2\ddot{\varphi}l_r] \\ \\ m_s[\ddot{Z}_{CGS} - l_s(\ddot{\psi}\cos\theta - \dot{\psi}\dot{\theta}\sin\theta] + m_{usf}[\ddot{Z}_{usfL} + \\ \ddot{Z}_{usfR} - 2\dot{\omega}_w l_f\cos\delta_f] + m_{usr}[\ddot{Z}_{usrL} + \ddot{Z}_{usrR} - 2\dot{\omega}_w l_r] \end{Bmatrix} \quad (13) $$

Which, $m = m_s + 2m_{usf} + 2m_{usr}$ is the total mass of the vehicle. According to Newton's angular momentum equation, the resultant of the torques acting on the body is equal to the change of the body's angular momentum. If we write this relation for the center of the vehicle coordinate system whose distance to the center of the sprung mass coordinate system remains constant, "Eq. (14)" will be obtained:

$$ {}^{V}\mathbf{M}_S = {}^{V}_{S}\mathbf{R}\,{}^{S}\mathbf{M}_S = {}^{V}_{S}\mathbf{R}\frac{d}{dt}\left({}^{S}\mathbf{I}_S\,{}^{S}\boldsymbol{\omega}_S\right) \quad (14) $$

Which, ${}^{V}_{S}\mathbf{R}$ is the matrix of coordinate transformation from the sprung mass coordinates to the vehicle coordinates (see appendix). Assuming that the amounts of inertia moments remain constant with small rotation of roll and pitch of the vehicle, "Eq. (15)" is obtained:

$$ {}^{V}\mathbf{M}_S = {}^{V}\mathbf{I}_S\,{}^{V}\dot{\boldsymbol{\omega}}_S + {}^{V}\boldsymbol{\omega}_S\times\left({}^{V}\mathbf{I}_S\,{}^{V}\boldsymbol{\omega}_S\right) \quad (15) $$

Where:

$$ {}^{V}\dot{\boldsymbol{\omega}}_S = \frac{d}{dt}{}^{V}\boldsymbol{\omega}_S + {}^{V}\boldsymbol{\omega}_V\times{}^{V}\boldsymbol{\omega}_S = \begin{Bmatrix} \ddot{\theta} - \dot{\varphi}\dot{\psi}\cos\theta \\ \ddot{\psi}\cos\theta - \dot{\psi}\dot{\theta}\sin\theta + \dot{\theta}\dot{\varphi} \\ \ddot{\varphi} + \ddot{\psi}\sin\theta + \dot{\psi}\dot{\theta}\cos\theta \end{Bmatrix} \quad (16) $$

Since the xy plane is symmetry plane of the vehicle with a good approximation, so $I_{xy} = I_{yz} = 0$ and with ignoring the value of I_{xz}, the matrix of sprung mass inertia moments will be presented in "Eq. (17)":

$$ {}^{V}\mathbf{I}_S = \begin{bmatrix} I_{xx} & I_{xy} & I_{xz} \\ I_{yx} & I_{yy} & I_{yz} \\ I_{zx} & I_{zy} & I_{zz} \end{bmatrix} \rightarrow {}^{V}\mathbf{I}_S = \begin{bmatrix} I_{xx} & 0 & 0 \\ 0 & I_{yy} & 0 \\ 0 & 0 & I_{zz} \end{bmatrix} \quad (17) $$

By placing ${}^{V}\boldsymbol{\omega}_s$, ${}^{V}\dot{\boldsymbol{\omega}}_e$ and ${}^{V}\mathbf{I}_s$, respectively, from "Eqs. (2), (16) and (17)" in the "Eq. (15)", "Eq. (18)" is obtained:

$$ {}^{V}\mathbf{M}_S = \begin{Bmatrix} I_{xx}\left(\ddot{\theta} - \dot{\varphi}\dot{\psi}\cos\theta\right) + \\ \left(I_{zz} - I_{yy}\right)\left(\dot{\varphi}\dot{\psi}\cos\theta + \dot{\psi}^2\sin\theta\cos\theta\right) \\ I_{yy}\left(\ddot{\psi}\cos\theta - \dot{\theta}\dot{\psi}\sin\theta + \dot{\theta}\dot{\varphi}\right) + \\ \left(I_{xx} - I_{zz}\right)\left(\dot{\psi}\dot{\theta}\sin\theta + \dot{\theta}\dot{\varphi}\right) \\ I_{zz}\left(\ddot{\varphi} + \ddot{\psi}\sin\theta + \dot{\theta}\dot{\psi}\cos\theta\right) + \\ \left(I_{yy} - I_{xx}\right)\dot{\psi}\dot{\theta}\cos\theta \end{Bmatrix} \quad (18) $$

To derive the equation of unsprung mass angular momentum, similar to the equation of sprung mass

angular momentum ("Eq. (15)"), "Eqs. (19-21)" are obtained as follows:

$$ {}^{V}\mathbf{M}_{usij} = {}^{V}\mathbf{I}_{usij}\,{}^{V}\dot{\boldsymbol{\omega}}_{usij} + {}^{V}\boldsymbol{\omega}_{usij} \times \left({}^{V}\mathbf{I}_{usij}\,{}^{V}\boldsymbol{\omega}_{usij} \right) \tag{19} $$

$$ {}^{V}\dot{\boldsymbol{\omega}}_{usij} = \frac{d}{dt}\,{}^{V}\boldsymbol{\omega}_{usij} + {}^{V}\boldsymbol{\omega}_{V} \times {}^{V}\boldsymbol{\omega}_{usij} \rightarrow $$

$$ {}^{V}\dot{\boldsymbol{\omega}}_{usfR} = \begin{Bmatrix} \dot{\omega}_w \sin\delta_{fR} - \dot{\varphi}\omega_w \cos\delta_{fR} \\ \dot{\omega}_w \cos\delta_{fR} + \dot{\varphi}\omega_w \sin\delta_{fR} \\ \ddot{\varphi} \end{Bmatrix}, $$

$$ {}^{V}\dot{\boldsymbol{\omega}}_{usfL} = \begin{Bmatrix} \dot{\omega}_w \sin\delta_{fL} - \dot{\varphi}\omega_w \cos\delta_{fL} \\ \dot{\omega}_w \cos\delta_{fL} + \dot{\varphi}\omega_w \sin\delta_{fL} \\ \ddot{\varphi} \end{Bmatrix}, \tag{20} $$

$$ {}^{V}\dot{\boldsymbol{\omega}}_{usrL} = \begin{Bmatrix} -\dot{\varphi}\omega_w \\ \dot{\omega}_w \\ \ddot{\varphi} \end{Bmatrix}, {}^{V}\dot{\boldsymbol{\omega}}_{usrR} = \begin{Bmatrix} -\dot{\varphi}\omega_w \\ \dot{\omega}_w \\ \ddot{\varphi} \end{Bmatrix} $$

$$ {}^{V}\mathbf{M}_{usfR} = \begin{Bmatrix} I_{xxusf}\left(\dot{\omega}_w \sin\delta_{fR} - \dot{\varphi}\omega_w \cos\delta_{fR}\right) + \\ \left(I_{zzusf} - I_{yyusf}\right)\dot{\varphi}\omega_w \cos\delta_{fR} \\ I_{yyusf}\left(\dot{\omega}_w \cos\delta_{fR} + \dot{\varphi}\omega_w \sin\delta_{fR}\right) + \\ \left(I_{xxusf} - I_{zzusf}\right)\dot{\varphi}\omega_w \sin\delta_{fR} \\ I_{zzusf}\ddot{\varphi} + \left(I_{yyusf} - I_{xxusf}\right)\omega_w^2 \sin\delta_{fR}\cos\delta_{fR} \end{Bmatrix} $$

$$ {}^{V}\mathbf{M}_{usfL} = \begin{Bmatrix} I_{xxusf}\left(\dot{\omega}_w \sin\delta_{fL} - \dot{\varphi}\omega_w \cos\delta_{fL}\right) + \\ \left(I_{zzusf} - I_{yyusf}\right)\dot{\varphi}\omega_w \cos\delta_{fL} \\ I_{yyusf}\left(\dot{\omega}_w \cos\delta_{fL} + \dot{\varphi}\omega_w \sin\delta_{fL}\right) + \\ \left(I_{xxusf} - I_{zzusf}\right)\dot{\varphi}\omega_w \sin\delta_{fL} \\ I_{zzusf}\ddot{\varphi} + \left(I_{yyusf} - I_{xxusf}\right)\omega_w^2 \sin\delta_{fL}\cos\delta_{fL} \end{Bmatrix} \tag{21} $$

$$ {}^{V}\mathbf{M}_{usrL} = \begin{Bmatrix} -I_{xxusr}\dot{\varphi}\omega_w + \left(I_{zzusr} - I_{yyusr}\right)\dot{\varphi}\omega_w \\ I_{yyusr}\dot{\omega}_w \\ I_{zzusr}\ddot{\varphi} \end{Bmatrix} $$

$$ {}^{V}\mathbf{M}_{usrR} = \begin{Bmatrix} -I_{xxusr}\dot{\varphi}\omega_w + \left(I_{zzusr} - I_{yyusr}\right)\dot{\varphi}\omega_w \\ I_{yyusr}\dot{\omega}_w \\ I_{zzusr}\ddot{\varphi} \end{Bmatrix} $$

Considering that the center of coordinate of the vehicle is a point that differs from the center of mass of the sprung and unsprung masses, according to "Eq. (22)", the total torque applied to the vehicle can be calculated [18]:

$$ \left(\mathbf{H}_Q\right)_{rel} = \left(\mathbf{H}_G\right)_{rel} + \bar{\boldsymbol{\rho}} \times m\mathbf{V}_{rel} \tag{22} $$

Equation (22) shows the angular torque around the desired point Q. According to the toques principle in which the sum of the torques of all external forces of the system around of point Q must be equal to resultant their torque around Q, "Eq. (23)" is obtained as follows:

$$ \sum \mathbf{M}_Q = \sum \mathbf{M}_G + \bar{\boldsymbol{\rho}} \times \sum \mathbf{F} \tag{23} $$

By placing vector of forces and torques in "Eq. (23)" for the proposed vehicle model, "Eq. (24)" is obtained:

$$ {}^{V}\mathbf{M}_V = {}^{V}\mathbf{M}_S + {}^{V}\mathbf{M}_{usij} + {}^{V}\boldsymbol{\rho}_{CGS} \times {}^{V}\mathbf{F}_S + {}^{V}\boldsymbol{\rho}_{usij} \times {}^{V}\mathbf{F}_{usij} \tag{24} $$

By exerting the force-torque equations ("Eqs. (7), (9-12), (18) and (21)") in "Eq. (24)", torque components of the vehicle are obtained according to "Eqs. (25-27)":

$$ \begin{aligned} &{}^{V}M_{VX} = I_{xx}\left(\ddot{\theta} - \dot{\varphi}\dot{\psi}\cos\theta\right) + \\ &\left(I_{zz} - I_{yy}\right)\left(\dot{\varphi}\dot{\psi}\cos\theta + \dot{\psi}^2 \sin\theta\cos\theta\right) + \\ &2I_{xxusf}\left(\dot{\omega}_w \sin\delta_f - \dot{\varphi}\omega_w \cos\delta_f\right) + \\ &2\left(I_{zzusf} - I_{yyusf}\right)\dot{\varphi}\omega_w \cos\delta_f - 2I_{xxusr}\dot{\varphi}\omega_w + \\ &2\left(I_{zzusr} - I_{yyusr}\right)\dot{\varphi}\omega_w - \\ &m_s h_s[\dot{V}_y - h_s\ddot{\theta} + l_s\left(\ddot{\varphi} + \ddot{\psi}\sin\theta + \dot{\psi}\dot{\theta}\cos\theta\right) + \\ &\dot{\varphi}\left(V_x + h_s\dot{\psi}\cos\theta\right)] + \\ &(t/2)[m_{usf}(\ddot{Z}_{usfR} - \ddot{Z}_{usfL} + \dot{\omega}_w t\sin\delta_f) + \\ &m_{usf}(\ddot{Z}_{usrR} - \ddot{Z}_{usrL} + \dot{\omega}_w t)] - m_{usf}[Z_{usfR}(\dot{V}_y - \\ &\sin\delta_f(\dot{Z}_{usfR}\omega_w + Z_{usfR}\dot{\omega}_w) + l_f\ddot{\varphi} + \\ &\dot{\varphi}(V_x + Z_{usfR}\omega_w\cos\delta_f - (t/2)\dot{\varphi})) + \\ &Z_{usfL}(\dot{V}_y - \sin\delta_f(\dot{Z}_{usfL}\omega_w + Z_{usfL}\dot{\omega}_w) + \\ &l_f\ddot{\varphi} + \dot{\varphi}(V_x + Z_{usfL}\omega_w\cos\delta_f + (t/2)\dot{\varphi}))] - \\ &m_{usr}[Z_{usrL}(\dot{V}_y - \dot{Z}_{usrL}\omega_w - Z_{usrL}\dot{\omega}_w + \\ &l_r\ddot{\varphi} + \dot{\varphi}(V_x + Z_{usrL}\omega_w + (t/2)\dot{\varphi})) + \\ &Z_{usrR}(\dot{V}_y - \dot{Z}_{usrR}\omega_w - Z_{usrR}\dot{\omega}_w + \\ &l_r\ddot{\varphi} + \dot{\varphi}(V_x + Z_{usrR}\omega_w - (t/2)\dot{\varphi}))] \end{aligned} \tag{25} $$

$$ \begin{aligned} &{}^{V}M_{VY} = I_{yy}(\ddot{\psi}\cos\theta - \dot{\theta}\dot{\psi}\sin\theta + \dot{\theta}\dot{\varphi}) + \\ &(I_{xx} - I_{zz})(\dot{\psi}\dot{\theta}\sin\theta + \dot{\theta}\dot{\varphi}) + \\ &2I_{yyusf}\left(\dot{\omega}_w\cos\delta_f + \dot{\varphi}\omega_w\sin\delta_f\right) + \end{aligned} \tag{26} $$

$$
\begin{aligned}
&2\left(I_{xxusf}-I_{zzusf}\right)\dot{\varphi}\omega_w\sin\delta_f+\\
&2I_{yyusr}\dot{\omega}_w+m_s h_s[\dot{V}_x+h_s\ddot{\psi}\cos\theta-\\
&h_s\dot{\psi}\dot{\theta}\sin\theta+l_s\left(\ddot{\varphi}+\ddot{\psi}\sin\theta+\dot{\psi}\dot{\theta}\cos\theta\right)-\\
&\dot{\varphi}(V_y-h_s\dot{\theta}+l_s(\dot{\varphi}+\dot{\psi}\sin\theta))]-\\
&m_s l_s(\ddot{Z}_{CGS}-l_s\ddot{\psi}\cos\theta+l_s\dot{\psi}\dot{\theta}\sin\theta)+\\
&m_{usf}l_f[2l_f\dot{\omega}_w\cos\delta_f-\ddot{Z}_{usfR}-\ddot{Z}_{usfL}]+\\
&m_{usr}l_r[2l_r\dot{\omega}_w-\ddot{Z}_{usrR}-\ddot{Z}_{usrL}]+m_{usf}[Z_{usfR}[\dot{V}_x+\\
&\cos\delta_f(\dot{Z}_{usfR}\omega_w+Z_{usfR}\dot{\omega}_w)-(t/2)\ddot{\varphi}-\\
&\dot{\varphi}(V_y-Z_{usfR}\omega_w\sin\delta_f+l_f\dot{\varphi})]+\\
&[Z_{usfL}[\dot{V}_x+\cos\delta_f(\dot{Z}_{usfL}\omega_w+Z_{usfL}\dot{\omega}_w)+(t/2)\ddot{\varphi}-\\
&\dot{\varphi}(V_y-Z_{usfL}\omega_w\sin\delta_f+l_f\dot{\varphi})]]+m_{usr}[Z_{usrL}[\dot{V}_x+\dot{Z}_{usrL}\omega_w+\\
&Z_{usrL}\dot{\omega}_w+(t/2)\ddot{\varphi}-\dot{\varphi}(V_y-Z_{usrL}\omega_w+l_r\dot{\varphi})]+\\
&[Z_{usrR}[\dot{V}_x+\dot{Z}_{usrR}\omega_w+Z_{usrR}\dot{\omega}_w-\\
&(t/2)\ddot{\varphi}-\dot{\varphi}(V_y-Z_{usrR}\omega_w+l_r\dot{\varphi})]]
\end{aligned}
$$

$$
\begin{aligned}
&{}^{V}M_{VZ}=I_{zz}\left(\ddot{\varphi}+\ddot{\psi}\sin\theta+\dot{\theta}\dot{\psi}\cos\theta\right)+\left(I_{yy}-I_{xx}\right)\dot{\psi}\dot{\theta}\cos\theta+\\
&2I_{zzusf}\ddot{\varphi}+2(I_{yyusf}-I_{xxusf})\omega_w^2\sin\delta_f\cos\delta_f+2I_{zzusr}\ddot{\varphi}+\\
&m_s l_s(\dot{V}_y-h_s\ddot{\theta}+l_s(\ddot{\varphi}+\ddot{\psi}\sin\theta+\dot{\psi}\dot{\theta}\cos\theta+\\
&h_s\dot{\psi}\dot{\varphi}\cos\theta+\dot{\varphi}\dot{V}_x)+m_{usf}[l_f[2\dot{V}_y-\\
&\sin\delta_f((\dot{Z}_{usfR}+\dot{Z}_{usfL})\omega_w+(Z_{usfR}+Z_{usfL})\dot{\omega}_w)+\\
&2l_f\ddot{\varphi}+\dot{\varphi}(2V_x+\omega_w\cos\delta_f(Z_{usfR}+Z_{usfL}))]+\\
&(t/2)[\cos\delta_f(\omega_w(\dot{Z}_{usfR}+\dot{Z}_{usfL})+\dot{\omega}_w(Z_{usfR}+Z_{usfL}))+\\
&t\ddot{\varphi}-\dot{\varphi}\omega_w\sin\delta_f(Z_{usfR}-Z_{usfL})]]+\\
&m_{usr}[l_r[2\dot{V}_y-(\dot{Z}_{usrR}+\dot{Z}_{usrL})\omega_w+(Z_{usrR}+Z_{usrL})\dot{\omega}_w+\\
&2l_r\ddot{\varphi}+\dot{\varphi}(2V_x+\omega_w(Z_{usrR}+Z_{usrL}))]+\\
&(t/2)[\omega_w(\dot{Z}_{usrL}-\dot{Z}_{usrR})+\dot{\omega}_w(Z_{usrL}-Z_{usrR})+t\ddot{\varphi}-\\
&\dot{\varphi}\omega_w(Z_{usrR}-Z_{usrL})]]
\end{aligned}
\tag{27}
$$

The left side of "Eqs. (13) and (25-27)", which are the main equations of motion of the vehicle, includes the forces and torques of the external forces applied to the vehicle and an example of them is shown in "Fig. 2". By considering the directions of the coordinate systems, these forces and torques are entered into the equations of motion of the vehicle.

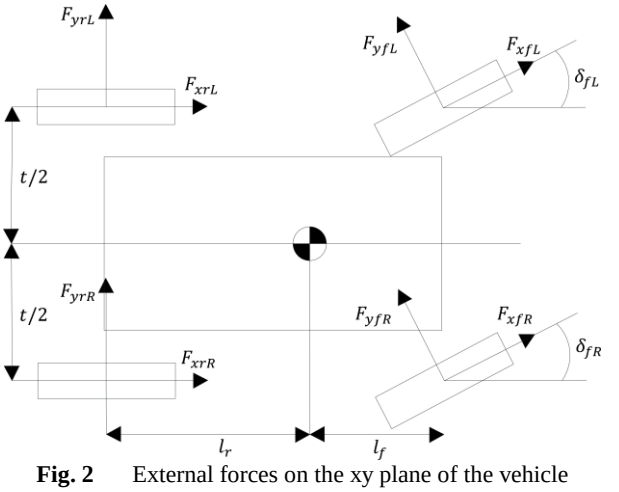

Fig. 2 External forces on the xy plane of the vehicle coordinate system.

2.1. Equations of External Forces

By writing the resultant of forces and torques applied to the vehicle, "Eqs. (28) and (29)" are obtained:

$$
{}^{V}\mathbf{F}_V=\begin{Bmatrix}
F_{xfR}\cos\delta_{fR}-F_{yfR}\sin\delta_{fR}+F_{xfL}\cos\delta_{fL}-\\
F_{yfL}\sin\delta_{fL}+F_{xrR}+F_{xrL}\\
F_{yfR}\cos\delta_{fR}+F_{xfR}\sin\delta_{fR}+F_{yfL}\cos\delta_{fL}+\\
F_{xfL}\sin\delta_{fL}+F_{yrR}+F_{yrL}\\
m_s g-k_{ij}\left(Z_n-Z_{usij}\right)-c_{ij}\left(\dot{Z}_n-\dot{Z}_{usij}\right)
\end{Bmatrix}
\tag{28}
$$

$$
{}^{V}\mathbf{M}_V=\begin{Bmatrix}
(t/2)[-k_{fR}\left(Z_1-Z_{usfR}\right)-k_{rR}\left(Z_4-Z_{usrR}\right)+\\
k_{fL}\left(Z_2-Z_{usfL}\right)+k_{rL}\left(Z_3-Z_{usrL}\right)-\\
c_{fR}\left(\dot{Z}_1-\dot{Z}_{usfR}\right)-c_{rR}\left(\dot{Z}_4-\dot{Z}_{usrR}\right)+\\
c_{fL}\left(\dot{Z}_2-\dot{Z}_{usfL}\right)+c_{rL}\left(\dot{Z}_3-\dot{Z}_{usrL}\right)]+\\
h_{RCf}(F_{yfR}\cos\delta_{fR}+F_{xfR}\sin\delta_{fR}+\\
F_{yfL}\cos\delta_{fL}+F_{xfL}\sin\delta_{fL})+\\
h_{RCr}(F_{yrR}+F_{yrL})+m_s g h_s\sin\theta\\
\\
l_f[k_{fR}\left(Z_1-Z_{usfR}\right)+k_{fL}\left(Z_2-Z_{usfL}\right)]-\\
l_r[k_{rR}\left(Z_4-Z_{usrR}\right)+k_{rL}\left(Z_3-Z_{usrL}\right)]+\\
l_f[c_{fR}\left(\dot{Z}_1-\dot{Z}_{usfR}\right)+c_{fL}\left(\dot{Z}_2-\dot{Z}_{usfL}\right)]-\\
l_r[c_{rR}\left(\dot{Z}_4-\dot{Z}_{usrR}\right)+c_{rL}\left(\dot{Z}_3-\dot{Z}_{usrL}\right)]-\\
m_s g l_s\cos\psi+h_{RA}(F_{xfR}\cos\delta_{fR}-F_{yfR}\sin\delta_{fR}+\\
F_{xfL}\cos\delta_{fL}-F_{yfL}\sin\delta_{fL}+F_{xrR}+F_{xrL})\\
\\
(t/2)(-F_{xfR}\cos\delta_{fR}+F_{yfR}\sin\delta_{fR}+\\
F_{xfL}\cos\delta_{fL}-F_{yfL}\sin\delta_{fL}-F_{xrR}+F_{xrL})-\\
l_f(F_{yfR}\cos\delta_{fR}+F_{xfR}\sin\delta_{fR}+F_{yfL}\cos\delta_{fL}+\\
F_{xfL}\sin\delta_{fL})+l_r\left(F_{yrR}+F_{yrL}\right)
\end{Bmatrix}
\tag{29}
$$

In "Eqs. (28) and (29)", Z_n is the displacement of a point of the sprung mass in the vertical direction above the unsprung masses, which is calculated according to "Eq. (30)":

$$\begin{aligned} Z_1 &= Z_{CGS} + (t/2)\sin\theta - l_f \sin\psi \,, \\ Z_2 &= Z_{CGS} - (t/2)\sin\theta - l_f \sin\psi \,, \\ Z_3 &= Z_{CGS} - (t/2)\sin\theta + l_r \sin\psi \,, \\ Z_4 &= Z_{CGS} + (t/2)\sin\theta + l_r \sin\psi \end{aligned} \tag{30}$$

2.2. Equations of Engine Rotating

Generally, in the extraction of equations of the vehicle, the sprung mass is considered as rigid. Now, if a part of the sprung mass has a rotation relative to the vehicle coordinate system (such as the engine crankshaft), then it is necessary to enter the effect of the rotation of this component in the force-torque equations that have been calculated so far. In this study, it is assumed that the rotating components are symmetric, so the product of inertia multiplications is zero. In this case, the rotation of these components will not create any force and therefore the force equation remains stable. However, if the rotational velocity of the rotating components or their moment of inertia is significant, then the gyroscopic moments due to the angular momentum of the rotating component are considerable and its effect must be considered in the torque equation. The gyroscopic moment is obtained according to "Eq. (31)":

$$\sum \mathbf{M} = \left(\frac{d\mathbf{H}}{dt}\right)_S + {}^V\boldsymbol{\omega}_s \times \mathbf{H} \,,\ \mathbf{H} = {}^V\mathbf{I}_e\, {}^V\boldsymbol{\omega}_e \tag{31}$$

In "Eq. (31)", **H** is the angular momentum vector of the engine and the vector of the angular velocity of the engine in the vehicle coordinate system ($^V\boldsymbol{\omega}_e$) is considered according to "Eq. (32)":

$${}^V\boldsymbol{\omega}_e = \left\{\dot{\theta} \quad \dot{\psi}\cos\theta + \omega_e \quad \dot{\phi} + \dot{\psi}\sin\theta\right\}^T \tag{32}$$

In this study, the crankshaft coordinate axes are considered to correspond to the vehicle coordinate axes, in which case the product of the crankshaft inertia multiplications in the vehicle coordinates is also equal to zero. Thus:

$${}^V\mathbf{I}_e = \begin{bmatrix} I_e & 0 & 0 \\ 0 & I_{ae} & 0 \\ 0 & 0 & I_e \end{bmatrix} \tag{33}$$

By placing "Eqs. (32) and (33)" in "Eq. (31)", the gyroscopic moment vector in the vehicle coordinate system is obtained as "Eq. (34)":

$${}^V\mathbf{M}_{Ve} = \begin{Bmatrix} I_e\left(\ddot{\theta} + \dot{\psi}^2\cos\theta\sin\theta + \dot{\phi}\dot{\psi}\cos\theta\right) - \\ I_{ae}\left(\dot{\psi}\cos\theta + \omega_e\right)\left(\dot{\psi}\sin\theta + \dot{\phi}\right) \\ I_{ae}\left(\ddot{\psi}\cos\theta - \dot{\theta}\dot{\psi}\sin\theta + \dot{\omega}_e\right) \\ I_e\left(\ddot{\phi} + \ddot{\psi}\sin\theta\right) + I_{ae}\dot{\theta}\left(\dot{\psi}\cos\theta + \omega_e\right) \end{Bmatrix} \tag{34}$$

In "Eq. (34)", ω is the angular velocity of the engine and I_{ae} is the crankshaft inertia moment around its rotation axis. In this study, the gyroscopic moment of the crankshaft is considered like other external torques and is added directly to the torque vector of external forces.

2.3. Wheels Equations of Motion

The wheel equations of motion in the vertical direction are determined according to "Eqs. (35-38)". With writing the resultant of the forces for each of the unsprung masses ("Fig. 3"), "Eqs. (35-38)" are obtained:

$$\begin{aligned} &\textstyle\sum F_z = m_{usij}\ddot{Z}_{usij} \rightarrow \\ &k_{fR}\left(Z_1 - Z_{usfR}\right) + c_{fR}\left(\dot{Z}_1 - \dot{Z}_{usfR}\right) + m_{usf}\,g - \\ &k_{tf}\left(Z_{usfR} - Z_{gfR}\right) - c_{tf}\left(\dot{Z}_{usfR} - \dot{Z}_{gfR}\right) = m_{usf}\ddot{Z}_{usfR} \end{aligned} \tag{35}$$

$$\begin{aligned} &k_{fL}\left(Z_2 - Z_{usfL}\right) + c_{fL}\left(\dot{Z}_2 - \dot{Z}_{usfL}\right) + m_{usf}\,g - \\ &k_{tf}\left(Z_{usfL} - Z_{gfL}\right) - c_{tf}\left(\dot{Z}_{usfL} - \dot{Z}_{gfL}\right) = m_{usf}\ddot{Z}_{usfL} \end{aligned} \tag{36}$$

$$\begin{aligned} &k_{rL}\left(Z_3 - Z_{usrL}\right) + c_{rL}\left(\dot{Z}_3 - \dot{Z}_{usrL}\right) + m_{usr}\,g - \\ &k_{tr}\left(Z_{usrL} - Z_{grL}\right) - c_{tr}\left(\dot{Z}_{usrL} - \dot{Z}_{grL}\right) = m_{usr}\ddot{Z}_{usrL} \end{aligned} \tag{37}$$

$$\begin{aligned} &k_{rR}\left(Z_4 - Z_{usrR}\right) + c_{rR}\left(\dot{Z}_4 - \dot{Z}_{usrR}\right) + m_{usr}\,g - \\ &k_{tr}\left(Z_{usrR} - Z_{grR}\right) - c_{tr}\left(\dot{Z}_{usrR} - \dot{Z}_{grR}\right) = m_{usr}\ddot{Z}_{usrR} \end{aligned} \tag{38}$$

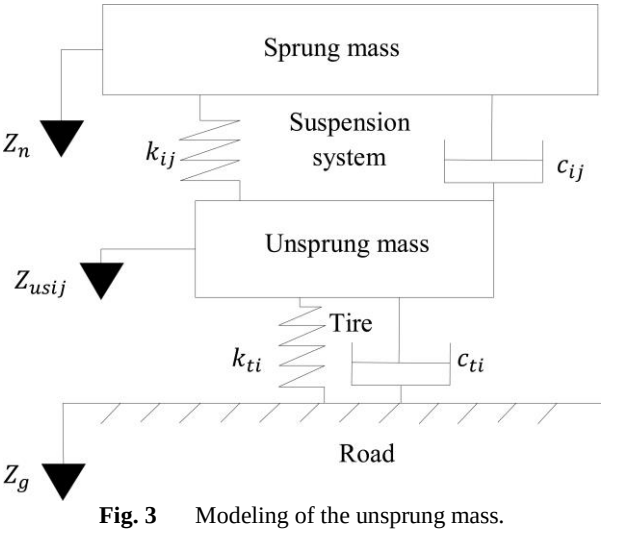

Fig. 3 Modeling of the unsprung mass.

2.4. Tire Modeling

In this research, the model of Pacejka 89 (Magic Formula), which has the ability to estimate the lateral and longitudinal forces of the tire under lateral and longitudinal slips, is considered [19-22]. This model receives variables such as vertical force of the wheel and longitudinal and lateral slips as input and its output is the longitudinal and lateral forces of the tire. The longitudinal slip is considered based on "Eqs. (39) and (40)":

Longitudinal slip during acceleration:

$$if \quad a_x > 0 \quad :\sigma = 1-(V_x/V_w) \tag{39}$$

Longitudinal slip during braking:

$$if \quad a_x < 0 \quad :\sigma = (V_w/V_x)-1 \tag{40}$$

In "Eqs. (39) and (40)", $V_w = r_w\omega_w$ and the lateral slip angle is difference between the direction of tire longitudinal axis and the direction of tire velocity vector in the xy plane ("Fig. 4"). The lateral slip angles are obtained in the form of "Eqs. (41) and (42)":

$$\begin{aligned}\alpha_{fR} &= \arctan\left[\left(V_y+\dot{\varphi}l_f\right)/\left(V_x+\dot{\varphi}(t/2)\right)\right]-\delta_f,\\ \alpha_{fL} &= \arctan\left[\left(V_y+\dot{\varphi}l_f\right)/\left(V_x-\dot{\varphi}(t/2)\right)\right]-\delta_f\end{aligned} \tag{41}$$

$$\begin{aligned}\alpha_{rR} &= \arctan\left[\left(V_y-\dot{\varphi}l_r\right)/\left(V_x+\dot{\varphi}(t/2)\right)\right],\\ \alpha_{rL} &= \arctan\left[\left(V_y-\dot{\varphi}l_r\right)/\left(V_x-\dot{\varphi}(t/2)\right)\right]\end{aligned} \tag{42}$$

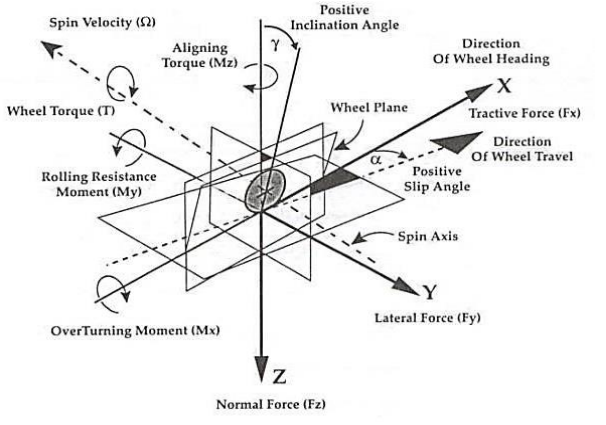

Fig. 4 Tire coordinates according to the SAE standard [19].

Therefore, the longitudinal and lateral forces of the tire are obtained according to "Eqs. (43) and (44)" by determining the longitudinal slip and lateral slip angle. In the appendix, the constants of Magic Formula (Pacejka 89) are given and longitudinal and lateral forces of Magic Formula are shown in "Figs. 5 and 6".

$$\begin{aligned}&F_x = D\sin\left(C\arctan\left(BX_1 - E\left(BX_1-\arctan\left(BX_1\right)\right)\right)\right)+Sv\\ &C=b_0,\ D=\left(b_1F_z^2+b_2F_z\right),\\ &BCD=\left(b_3F_z^2+b_4F_z\right)e^{\left(-b_5F_z\right)},\\ &B=BCD/(CD),\ E=\left(b_6F_z^2+b_7F_z+b_8\right),\\ &Sh=b_9F_z+b_{10},\ Sv=0,\ X_1=\sigma+Sh\end{aligned} \tag{43}$$

$$\begin{aligned}&F_y = D\sin\left(C\arctan\left(BX_1 - E\left(BX_1-\arctan\left(BX_1\right)\right)\right)\right)+Sv\\ &C=a_0,\ D=\left(a_1F_z^2+a_2F_z\right),\\ &BCD=a_3\sin\left(\arctan\left(F_z/a_4\right)\right)\left(1-a_5|\gamma|\right),\\ &B=BCD/(CD),\ E=\left(a_6F_z+a_7\right),\\ &Sh=a_9F_z+a_{10}+a_8\gamma,\ Sv=a_{11}F_z\gamma+a_{12}F_z+a_{13}\\ &,\\ &X_1=\alpha+Sh\end{aligned} \tag{44}$$

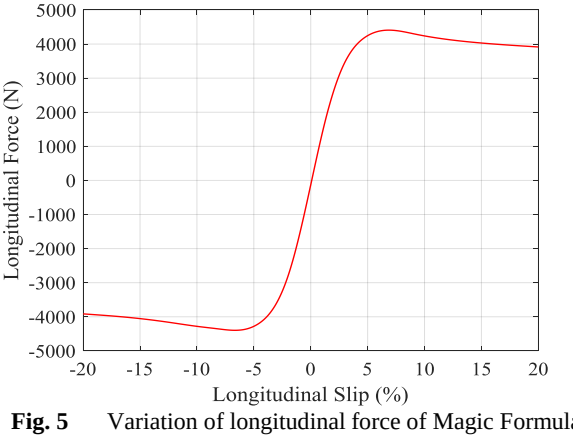

Fig. 5 Variation of longitudinal force of Magic Formula according to the longitudinal slip.

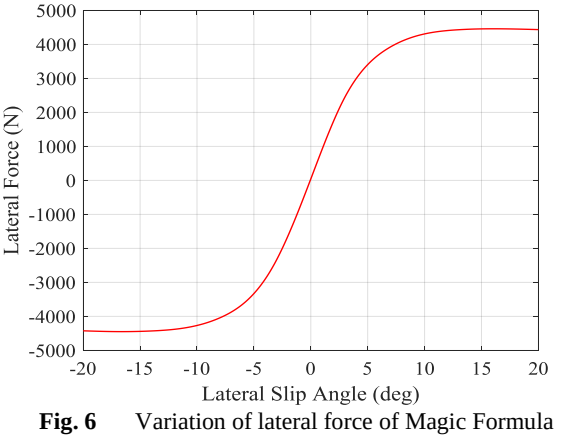

Fig. 6 Variation of lateral force of Magic Formula according to the lateral slip angle.

3 NUMERICAL METHOD

By using numerical method of the Newmark in the form of time integration [29], vehicle's dynamic behavior is simulated. In the Newmark family methods, at time of τ the vector of displacement ($\mathbf{q}$), velocity ($\dot{\mathbf{q}}$) and acceleration ($\ddot{\mathbf{q}}$) are estimated by $\mathbf{E}_{d+1}$, $\dot{\mathbf{E}}_{d+1}$ and $\mathbf{a}_{d+1}$ at time of τ_{d+1}. The vehicle's displacement vector is selected as "Eq. (45)" and the governing matrix-vector equations at time of $\tau = \tau_{d+1}$ can be changed to an estimated prescription as "Eq. (46)".

$$\mathbf{q} = \{X, Y, Z_{CGS}, \theta, \varphi, \psi, Z_{usfR}, Z_{usfL}, Z_{usrR}, Z_{usrL}\}^T \quad (45)$$

$$\begin{aligned} &\boldsymbol{\Gamma}(\mathbf{E}_{d+1})\mathbf{a}_{d+1} + \mathbf{G}(\mathbf{E}_{d+1}, \dot{\mathbf{E}}_{d+1}) = \boldsymbol{\Lambda}_{d+1} \\ &\mathbf{E}_0 = \mathbf{E}(0), \dot{\mathbf{E}}_0 = \dot{\mathbf{E}}(0), \mathbf{a}_0 = -\boldsymbol{\Gamma}^{-1}(\mathbf{E}(0))\mathbf{G}(\mathbf{E}(0), \dot{\mathbf{E}}(0)) \end{aligned} \quad (46)$$

Where, $\boldsymbol{\Gamma}$ is the inertia matrix and $\boldsymbol{\Gamma}$ and $\mathbf{G}$ are function of the displacement and velocity, $\boldsymbol{\Lambda}$ is the vector of external excitations, $\mathbf{E}_0$ is the initial displacement, $\dot{\mathbf{E}}_\mathbf{0}$ is the initial velocity and $\mathbf{a}_0$ is the initial acceleration. Displacement and velocity can be predicted by "Eqs. (47) and (48)":

$$\hat{\mathbf{E}}_d = \mathbf{E}_d + \Delta\tau\dot{\mathbf{E}}_d + 0.5\Delta\tau^2(1-2\xi)\mathbf{a}_d \quad (47)$$

$$\hat{\dot{\mathbf{E}}}_d = \dot{\mathbf{E}}_d + (1-\eta)\Delta\tau\mathbf{a}_d \quad (48)$$

Where, $\Delta\tau = \tau_{d+1} - \tau_d$ is the size of time step, ξ and η are the Newmark's algorithm parameters which show the accuracy of the algorithmic. Updated displacement and velocity are obtained from "Eqs. (49) and (50)":

$$\mathbf{E}_{d+1} = \hat{\mathbf{E}}_d + \xi\Delta\tau^2\mathbf{a}_{d+1} \quad (49)$$

$$\dot{\mathbf{E}}_{d+1} = \hat{\dot{\mathbf{E}}}_d + \eta\Delta\tau\mathbf{a}_{d+1} \quad (50)$$

In order to obtain $\mathbf{E}_{d+1}$ and $\dot{\mathbf{E}}_{d+1}$, update of the acceleration must be known ($\mathbf{a}_{d+1}$). By using method of the Newton–Raphson for every time step and by placing "Eqs. (49) and (50)" into "Eq. (46)", $\mathbf{a}_{d+1}$ is obtained from "Eqs. (51) and (52)":

$$\Delta\mathbf{a}^u_{d+1} + \mathbf{a}^u_{d+1} = \mathbf{a}^{u+1}_{d+1} \quad (51)$$

$$\mathbf{J}^u_{d+1}\Delta\mathbf{a}^u_{d+1} = -\boldsymbol{\Gamma}^u_{d+1}\mathbf{a}^u_{d+1} - \mathbf{G}^u_{d+1} + \boldsymbol{\Lambda}_{d+1} \quad (52)$$

Where, d and u are the iteration number of time step and Newton–Raphson method, $\boldsymbol{\Gamma}^u_{d+1} = \boldsymbol{\Gamma}(\mathbf{E}^u_{d+1})$, $\mathbf{G}^u_{d+1} = \mathbf{G}(\mathbf{E}^u_{d+1}, \dot{\mathbf{E}}^u_{d+1})$ and $\mathbf{J}^u_{d+1}$ is the matrix of Jacobian and is defined as "Eq. (53)":

$$\begin{aligned} \mathbf{J}^u_{d+1} = \boldsymbol{\Gamma}(\mathbf{E}^u_{d+1}) + \xi\Delta\tau^2\left[\frac{\partial\boldsymbol{\Gamma}^u_{d+1}\mathbf{a}^u_{d+1}}{\partial\mathbf{E}^u_{d+1}} + \frac{\partial\mathbf{G}^u_{d+1}}{\partial\mathbf{E}^u_{d+1}}\right] + \\ \eta\Delta\tau\frac{\partial\mathbf{G}^u_{d+1}}{\partial\dot{\mathbf{E}}^u_{d+1}}) \end{aligned} \quad (53)$$

4 VALIDATION AND SIMULATION RESULTS

Several different test programs in the phase IV of NHTSA's light vehicle rollover research program were reviewed and evaluated to select the most appropriate maneuver from them to investigate the rollover. According to "Table 1" , it can be seen that one of the best maneuvers, is the fishhook#1b, which has obtained the highest score. According to "Fig. 7" in the fishhook#1b test, the pause time of the hand-wheel angle (T1) at the maximum angle of the initial hand-wheel angle is until the roll rate of the vehicle reaches 1.5 degrees per second. On the other hand, in the fishhook#1b maneuver, the change of hand-wheel angle direction is done when the roll rate of the vehicle has reached 1.5 degrees per second.

Table 1 Comparison of different rollover maneuvers [2]

Assessment Criterion	NHTSA J-Turn	Fishhook #1a	Fishhook #1b	Nissan Fishhook
Objectivity and Repeatability	Excellent	Excellent	Excellent	Good
Performability	Excellent	Good	Excellent	Satisfactory
Discriminatory Capability	Excellent	Excellent	Excellent	Excellent
Appearance of Reality	Good	Excellent	Excellent	Good

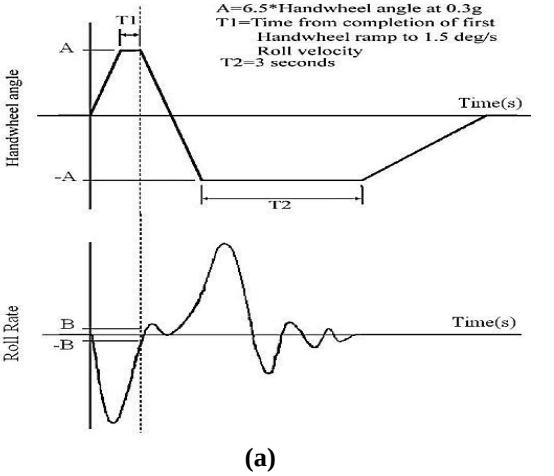

(a)

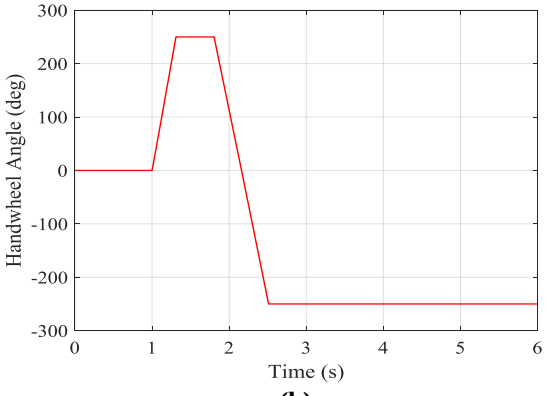

(b)

Fig. 7 Schematic of hand-wheel angle of the vehicle in: (a): NHTSA fishhook#1b maneuver [2], and (b): this study.

Due to the fact that the vehicle is assumed to be perfectly symmetrical with respect to its xz plane, direction of the hand-wheel angle (clockwise or counterclockwise) of "Fig. 7" has no effect on the maneuver results. The initial speed of the vehicle is shown in "Figs. 8 and 9" and the engine speed is 5000 revolutions per minute (RPM). During fishhook#1b maneuver, the passed trajectory by the vehicle is shown in "Fig. 10".

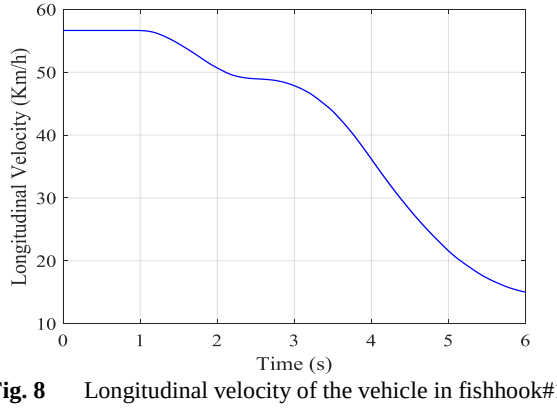

Fig. 8 Longitudinal velocity of the vehicle in fishhook#1b maneuver.

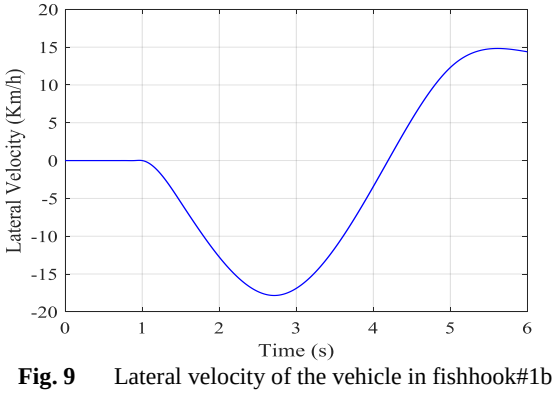

Fig. 9 Lateral velocity of the vehicle in fishhook#1b maneuver.

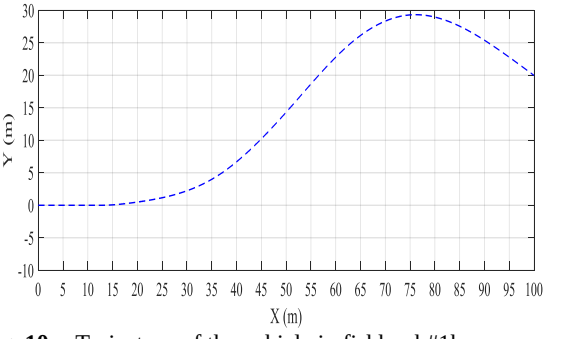

Fig. 10 Trajectory of the vehicle in fishhook#1b maneuver.

By applying the hand-wheel angle according to "Fig. 7", the numerical method of the Newmark and the parameters of "Table 2" , the dynamic behavior of the vehicle is compared by ADAMS/Car software according to "Figs. 11-13". Based on the validation results, it is found that the 15-DOF presented model in this research simulates the vehicle's dynamic behavior with a good accuracy. According to the results, by applying the steering input, the lateral acceleration reaches about 0.8g and after a few seconds decreases with decreasing longitudinal velocity of the vehicle. The roll angle of the vehicle reaches about 8.5 degrees and after a few oscillations due to the vibrational behavior of the system, it decreases. The maximum roll rate of the vehicle also reaches about 37 degrees per second.

Table 2 System parameters of this study

Parameter	Value	Unit	Parameter	Value	Unit
m_s	808	Kg	c_r	882.9	N.s/m
m_{usf}	2×31.5	Kg	I_x	298	Kg.m^2
m_{usr}	2×29.5	Kg	I_y	1243	Kg.m^2
h_{CG}	0.54	m	I_z	1130	Kg.m^2
h_{RA}	0.1	m	r_w	0.257	m
t	1.4	m	h_{RC}	0.1	m
l_f	0.945	m	h_s	0.45	m
l_r	1.4	m	I_{ae}	1.5	Kg.m^2
k_f	16	kN/m	k_{tf}	160	kN/m
k_r	15.4	kN/m	k_{tr}	154	kN/m
c_f	1414.3	N.s/m	ξ	0.25	-
c_t	0	N.s/m	η	0.5	-
l_s	0.35	m			

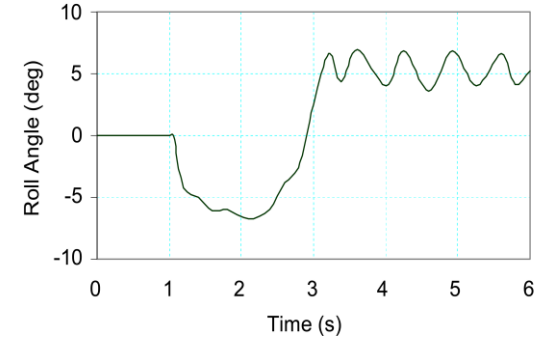

(a)

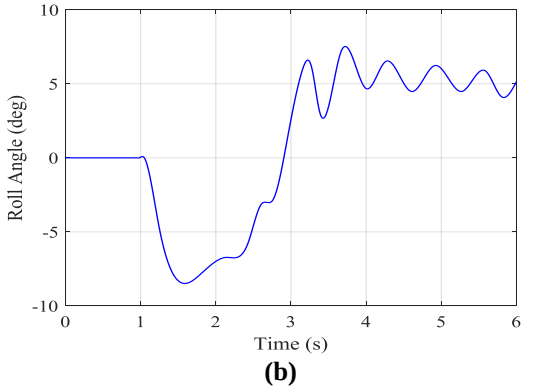

(b)

Fig. 11 Roll angle of the vehicle in fishhook#1b maneuver: (a): ADAMS software, and (b): this study.

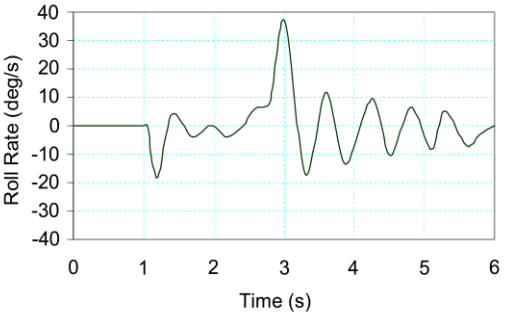

(a)

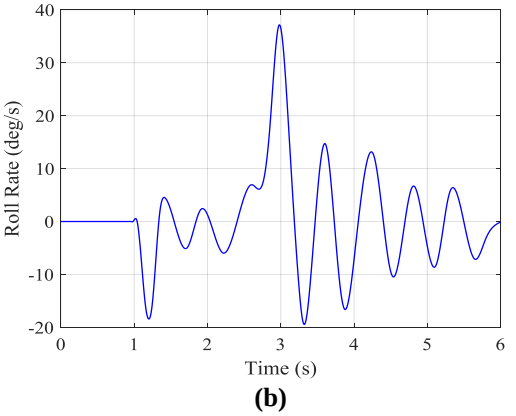

(b)

Fig. 12 Roll rate of the vehicle in fishhook#1b maneuver: (a) ADAMS software and (b) this study.

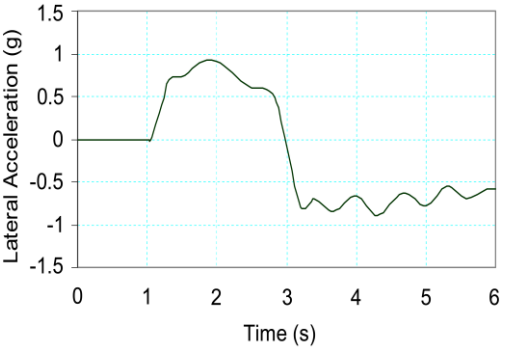

(a)

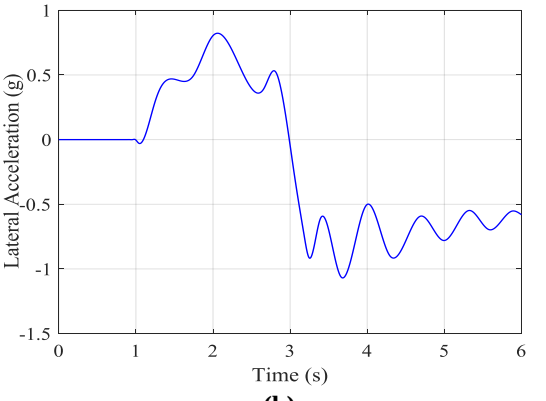

(b)

Fig. 13 Lateral acceleration of the vehicle in fishhook#1b maneuver: (a) ADAMS software and (b) this study.

5 CONCLUSION

This study presents the dynamics of a 15-DOF model of the vehicle by performing simulations to investigate the vehicle's dynamic behavior in fishhook maneuver under the supervision of the phase IV of NHTSA's light vehicle rollover research program. Using Newton's equations of motion, the equations of motion for the sprung and unsprung masses are all written in the vehicle coordinate system. In order to study the engine dynamics, the crankshaft coordinate axes are considered to correspond to the vehicle coordinate axes. Finally, the gyroscopic moment of the crankshaft is added directly to the torque vector of external forces, and the governing equations are evaluated by numerical method of the Newmark. The tire is modeled with the Pacejka 89 model, which estimates tire forces with using longitudinal and lateral slips. By selecting the fishhook#1b maneuver, the dynamic behavior of the 15-DOF presented model is validated by ADAMS/Car software. Based on the simulation results, it is found that the 15-DOF presented model in this research simulates the vehicle's dynamic behavior with a good accuracy. By applying the steering input, the lateral acceleration

reaches about 0.8g and after a few seconds decreases with decreasing longitudinal velocity of the vehicle. The roll angle of the vehicle reaches about 8.5 degrees and after a few oscillations due to the vibrational behavior of the system, it decreases. The maximum roll rate of the vehicle reaches about 37 degrees per second.

6 APPENDIX OR NOMENCLATURE

Nomenclature				Subscripts			
a	Acceleration and lateral constants of the Magic Formula	t	Track width	a	Crankshaft	s	Sprung mass
b	Longitudinal constants of the Magic Formula	V	Velocity	C	Center of gravity	t	Tire
c	Damping coefficient	Z	Vertical displacement	e	Engine	us	Unsprung mass
F	Force	Greek Letters		f	Front	V	Vehicle
h	Height	α	Lateral slip angle	g	Road	w	Wheel
H	Angular momentum	γ	Camber angle	i	Front and rear wheels (f,r)	x	Longitudinal direction
I	Moment of inertia	δ	Steering input	j	Right and left wheels (L,R)	y	Lateral direction
k	Stiffness coefficient	θ	Roll angle	L	Left side	z	Vertical direction
m	Mass	σ	Longitudinal slip	r	Rear		
M	Torque	φ	Yaw angle	R	Right side		
r	Radius	ψ	Pitch angle	$R.$	Roll axis		
R	Function of coordinate transformation	ω	Angular velocity	R	Roll center		

The transformation relation between coordinate systems of the sprung mass and vehicle which results from rotation of pitch and roll, is obtained as follows:

$$ {}^{v}_{s}\mathbf{R} = \begin{bmatrix} \cos\psi & 0 & \sin\psi \\ 0 & 1 & 0 \\ -\sin\psi & 0 & \cos\psi \end{bmatrix} \begin{bmatrix} 1 & 0 & 0 \\ 0 & \cos\theta & -\sin\theta \\ 0 & \sin\theta & \cos\theta \end{bmatrix} \rightarrow $$

$$ {}^{v}_{s}\mathbf{R} = \begin{bmatrix} \cos\psi & \sin\psi\sin\theta & \sin\psi\cos\theta \\ 0 & \cos\theta & -\sin\theta \\ -\sin\psi & \cos\psi\sin\theta & \cos\psi\cos\theta \end{bmatrix} $$

Table 3 Constant values used in the Pacejka 89 tire model

Lateral constants	Longitudinal constants
$a_0 = 1.65$, $a_1 = -34$, $a_2 = 1250$, $a_3 = 3036$, $a_4 = 12.8$, $a_5 = 0.00501$, $a_6 = -0.02103$, $a_7 = 0.77394$, $a_8 = 0.002289$, $a_9 = 0.013442$, $a_{10} = 0.003709$, $a_{11} = 19.1656$, $a_{12} = 1.21356$, $a_{13} = 6.26206$	$b_0 = 2.37272$, $b_1 = -9.46$, $b_2 = 1490$, $b_3 = 130$, $b_4 = 276$, $b_5 = 0.0886$, $b_6 = 0.00402$, $b_7 = -0.0615$, $b_8 = 1.2$, $b_9 = 0.0299$, $b_{10} = -0.176$

REFERENCES

[1] Heydinger, G. J., Howe, J.G., Analysis of Vehicle Response Data Measured During Severe Maneuvers, SAE Transactions, 2000, pp. 2154-2167.

[2] Forkenbrock, G. J., Garrott, W. R., Heitz, M., and O'Harra, B. C., A Comprehensive Experimental Examination of Test Maneuvers That May Induce on-Road, Untripped, Light Vehicle Rollover-Phase IV of NHTSA's Light Vehicle Rollover Research Program, Report DOT HS, Vol. 809, No. 513, 2002.

[3] Nalecz, A. G., Lu, Z., and Lu, Z., Methodology for Tripped Vehicle Rollover Testing and Analysis of Experimental Results, SAE Transactions, 1994, pp. 104-131.

[4] Allen, R. W., Szostak, H. T., Rosenthal, T. J., Klyde, D. H., and Owens, K. J., Characteristics Influencing Ground Vehicle Lateral/Directional Dynamic Stability, SAE Transactions, 1991, pp. 336-361.

[5] Zulhilmi, I. M., Peeie, M. H., Asyraf, S. M., Sollehudin, I. M., and Ishak, I. M., Experimental Study on the Effect of Emergency Braking Without Anti-Lock Braking System to Vehicle Dynamics Behavior, International Journal of Automotive and Mechanical Engineering, Vol. 17, No. 2, 2020, pp. 7832-7841.

[6] Ahmadian, M., Integrating Electromechanical Systems in Commercial Vehicles for Improved Handling, Stability, and Comfort, SAE International Journal of Commercial Vehicles, Vol. 7, 2014, pp. 535-587.

[7] Ataei, M., Khajepour, A., and Jeon, S., Model Predictive Control for Integrated Lateral Stability, Traction/Braking Control, and Rollover Prevention of Electric Vehicles, Vehicle System Dynamics, Vol. 58, No. 1, 2020, pp. 49-73.

[8] Phanomchoeng, G., Rajamani, R., New Rollover Index for the Detection of Tripped and Untripped Rollovers, IEEE Transactions on Industrial Electronics, Vol. 60, No. 10, 2012, pp. 4726-4736.

[9] Peng, Y., Chen, J., and Ma, Y., Observer-Based Estimation of Velocity and Tire-Road Friction Coefficient for Vehicle Control Systems, Nonlinear Dynamics, Vol. 96, No. 1, 2014, pp. 363-387.

[10] Yuvapriya, T., Lakshmi, P., and Rajendiran, S., Vibration Suppression in Full Car Active Suspension System Using Fractional Order Sliding Mode Controller, Journal of the Brazilian Society of Mechanical Sciences and Engineering, Vol. 40, No. 4, 2018.

[11] Papaioannou, G., Dineff, A. M., and Koulocheris, D., Comparative Study of Different Vehicle Models with Respect to Their Dynamic Behavior, International Journal of Automotive and Mechanical Engineering, Vol. 16, 2019, pp. 7061-7092.

[12] Mehrtash, M., Yuen, T., and Balan, L., Implementation of Experiential Learning for Vehicle Dynamic in Automotive Engineering: Roll-Over and Fishhook Test, Procedia Manufacturing, Vol. 32, 2019, pp. 768-774.

[13] Wang, F., Chen, Y., A Novel Active Rollover Prevention for Ground Vehicles Based on Continuous Roll Motion Detection, Journal of Dynamic Systems, Measurement, and Control, Vol. 141, No. 1, 2019.

[14] Zhang, H., Liang, J., Jiang, H., Cai, Y., and Xu, X., Stability Research of Distributed Drive Electric Vehicle by Adaptive Direct Yaw Moment Control, IEEE Access, Vol. **7**, 2019, pp. 106225-106237.

[15] Read, C., Viswanathan, H., An Aerodynamic Assessment of Vehicle-side Wall Interaction Using Numerical Simulation, International Journal of Automotive and Mechanical Engineering, Vol. 17, No. 1, 2020, pp. 7587-7598.

[16] Rajamani, R., Vehicle Dynamics and Control, Springer Science & Business Media, 2011.

[17] Gillespie, T. D., Fundamentals of Vehicle Dynamics, Society of Automotive Engineers Warrendale, Vol. 400, 1992.

[18] Meriam, J. L., Kraige, L. G., Engineering Mechanics: Dynamics, John Wiley & Sons, Vol. 2, 2012.

[19] Pacejka, H., Tire and Vehicle Dynamics, Elsevier, 2005.

[20] Bakker, E., Pacejka, H. B., and Lidner, L., A New Tire Model with an Application in Vehicle Dynamics Studies, SAE Transactions, 1989, pp. 101-113.

[21] Pacejka, H. B., Bakker, E., The Magic Formula Tyre Model, Vehicle System Dynamics, Vol. 21, No. S1, 1992, pp. 1-18.

[22] Bakker, E., Nyborg, L., and Pacejka, H. B., Tyre Modelling for Use in Vehicle Dynamics Studies, SAE Transactions, 1987, pp. 190-204.

[23] Lahmar, M., Frihi, D., and Nicolas, D., The Effect of Misalignment on Performance Characteristics of Engine Main Crankshaft Bearings, European Journal of Mechanics-A/Solids, Vol. 21, No. 4, 2002, pp. 703-714.

[24] Huang, T., Zhang, J., Chen, G., and Wang, C., Dynamic Balance Two-Dimensional Measuring of Crankshaft Assembly in Motorcycle Engine, IEEE Access, Vol. 8, 2020, pp. 133757-133766.

[25] Ahmadabadi, Z. N., Nonlinear Energy Transfer from an Engine Crankshaft to an Essentially Nonlinear Attachment, Journal of Sound and Vibration, Vol. 443, 2019, pp. 139-154.

[26] Mourelatos, Z. P., A Crankshaft System Model for Structural Dynamic Analysis of Internal Combustion Engines, Computers & Structures, Vol. 79, No. 20-21, 2001, pp. 2009-2027.

[27] Fonseca, L., De Faria, A., Crankshaft Deep Rolling Analysis Through Energy Balance Simulation Output, Journal of the Brazilian Society of Mechanical Sciences and Engineering, Vol. 41, No. 10, 2019.

[28] Drab, C. B., Engl, H. W., Haslinger, J. R., Offner, G., Pfau, R., and Zulehner, W., Dynamic Simulation of Crankshaft Multibody Systems, Multibody System Dynamics, Vol. 22, No. 2, 2009, pp. 133-144.

[29] Newmark, N. M., A Method of Computation for Structural Dynamics, Journal of the Engineering Mechanics Division, Vol. 85, No. 3, 1959, pp. 67-94.